NEUTRON STAR COOLING

By

WILLIAM THOMAS GRAHAM GLEN, B.Sc.

A Thesis

Submitted to the School of Graduate Studies

in Partial Fulfilment of the Requirements

for the Degree

Master of Science

McMaster University

October 1979

NEUTRON STAR COOLING

MASTER OF SCIENCE (1979) McMASTER UNIVERSITY
(Physics) Hamilton, Ontario

TITLE: Neutron Star Cooling

AUTHOR: William Thomas Graham Glen, B.Sc. (McGill)

SUPERVISOR: Dr. Peter G. Sutherland

NUMBER OF PAGES: v, 61

ABSTRACT

To determine the detectability of thermal radiation from the surface of a neutron star, the surface temperature as a function of time is needed. To find this, the surface temperature as a function of core temperature is found; this ratio depending on temperature, stellar mass, and magnetic field strength. The energy loss rates from photon emission and neutrino emission are calculated, along with the specific heat of the star; the latter two quantities depending on the core temperature. The surface temperature as a function of time is then calculated for various combinations of the variable parameters: stellar mass, equation of state, magnetic field, superfluidity, and pion cutoff density. Finally, a calculation of the detectability (distance vs. age) of a typical neutron star is made, using the estimated capabilities of the X-ray telescope on the Einstein Observatory.

ACKNOWLEDGEMENTS

I would like to thank my supervisor Dr. Peter Sutherland for introducing me to this topic, and for his words of wisdom without which I might never have finished. I have also enjoyed many interesting discussions with other members of the theory group, notably with Frank Hayes and with my dinner companion Axel Becke.

I also thank McMaster University for financial support these past two years.

Finally, my appreciation goes to Mrs. Helen Kennelly for typing this thesis faster than I believed possible.

TABLE OF CONTENTS

CHAPTER I

INTRODUCTION

The experimental evidence for neutron stars has grown enormously starting with the discovery of pulsars in 1967. Over one hundred and fifty pulsars have been found, and they are almost certainly rotating, magnetized neutron stars (for a review see Manchester and Taylor 1977). Also, X-ray bursters and compact sources in X-ray emitting binaries have been identified as neutron stars (see for example Joss and Rappaport 1976).

To learn more about neutron stars, it would be useful to observe direct surface radiation from them. This has yet to be achieved. From theoretical considerations, and from the spectra of X-ray bursters (van Paradijs 1978, 1979), neutron stars are found to have radii ~ 10 Km for the luminosity ($L = 4\pi R^2 \sigma T^4$) to compare to that of a main sequence star. Such a high surface temperature implies a spectrum strong in soft X-rays; therefore such radiation is looked for with X-ray detectors. These detectors must be taken above the Earth's atmosphere since it is opaque to X-rays. The recent launchings of the High Energy Astronomy Laboratory (HEAO) satellites are responsible for much of the current interest in neutron star cooling.

Neutron stars are believed to be formed in supernovas, with very high initial temperatures ($\sim 10^{11}$ K). As they have no internal energy sources, neutron stars will cool off monotonically with time until they are no longer detectable. The aim of the present work is to determine the temperature of a neutron star as a function of age; this is useful since the ages of certain pulsars and supernova remnants are known. The cooling rate is affected by certain parameters (mass, magnetic field), and is sensitive to some uncertain properties of high density matter (equation of state, superfluidity parameters, possible pion condensate); therefore observations of surface temperature and age should reveal information about the star in question and of high density matter in general.

Such calculations of cooling rates have been done previously (see for example, Tsuruta and Cameron 1966; Tsuruta 1974, 1978; Maxwell 1979), however, the present work attempts a more detailed and exact calculation. In this work the best available opacities, conductivities, specific heats, and neutrino emissivities are made use of. The effects of variation in the high-density equation of state and variation in mass are explored. General relativistic effects are included; they are of order unity in many cases. The equation of state in the outer layers is accurately treated (for non-magnetic stars). Also, realistic superfluidity estimates are used as

opposed to the extremes used by other authors.

The general assumptions made in solving the problem should be noted here: (i) the star is taken to be spherically symmetric (rotation is neglected; it introduces a small asymmetry); (ii) the structure of the star is unchanging in time; (iii) there are no energy sources (the star merely loses stored heat); and (iv) for stars with magnetic fields, the obviously unrealistic use of spherical symmetry is meant to simulate an 'average' effect, and so should be looked upon more as a qualitative calculation.

CHAPTER II

EQUATIONS OF STELLAR STRUCTURE

The general relativistic differential equations of stellar structure for a spherically symmetric star are (Thorne 1967):

a) Mass equation.

$$\frac{dm}{dr} = 4\pi r^2 \rho \quad . \tag{2.1}$$

Here m(r) is the mass interior to radius r.

b) Tolman-Oppenheimer-Volkoff equation of hydrostatic equilibrium

$$\frac{dP}{dr} = \frac{-G(\rho+P/c^2)(m+4\pi r^3 P/c^2)}{r^2(1-2Gm/rc^2)} \quad . \tag{2.2}$$

P is the pressure and ρc^2 is the total mass-energy density, including internal energy.

c) Source equation for the gravitational potential ϕ.

$$\frac{d\phi}{dr} = \frac{G(m+4\pi r^3 P/c^2)}{r^2 c^2 (1-2Gm/rc^2)} \tag{2.3}$$

d) Equations of energy generation at constant composition (no net nuclear reactions)

$$\frac{d(Le^{2\phi})}{dr} = - \frac{4\pi r^2 n e^{\phi}}{(1-2Gm/rc^2)^{1/2}} T \frac{ds}{dt} . \qquad (2.4)$$

Here $\frac{ds}{dt}$ is the rate of change of entropy per particle, and n is the number density of particles. Equation (2.4) states that the contribution to the energy flux from a spherical shell of radius r is determined by the rate of change of the heat content of the shell.

The luminosity L(r) is that measured locally by an observer at rest with respect to the star. The luminosity is given by

$$L(r) = L_{\gamma}(r) + L_{\nu}(r) \qquad (2.5)$$

where L_{γ} and L_{ν} are the photon and neutrino luminosities, respectively.

The second equation of energy generation is

$$\frac{d(L_{\nu}e^{2\phi})}{dr} = \frac{4\pi r^2 n e^{2\phi}}{(1-2Gm/rc^2)^{1/2}} q_{\nu} \qquad (2.6)$$

where q_{ν} is the neutrino emissivity per particle. The neutrinos are produced by a variety of mechanisms and, by virtue of their long mean free paths, escape directly from their point of production.

e) Equation of energy transport.

$$\frac{d(Te^{\phi})}{dr} = \frac{-3\kappa\rho L_\gamma e^{\phi}}{16\sigma T^3 4\pi r^2 (1-2Gm/rc^2)^{1/2}} \quad \text{(no convection)} \qquad (2.7)$$

or

$$\frac{dT}{dr} = \frac{\Gamma_2 - 1}{\Gamma_2} \frac{T}{P} \frac{dP}{dr} \quad \text{(convection)} \; . \qquad (2.8)$$

The lesser in magnitude of the two temperature gradients is used. (However, none of the neutron stars examined in this work have convective layers.)

The opacity κ (in cm^2-g^{-1}) in eqn. (2.7) is given by

$$\frac{1}{\kappa} = \frac{1}{\kappa_R} + \frac{1}{\kappa_c} \qquad (2.9)$$

where κ_R is the radiative opacity, and κ_c is the conductive opacity, which is inversely related to the thermal conductivity.

At high densities $\kappa_c << \kappa_R$, therefore $\kappa \approx \kappa_c$, and this decreases rapidly with increasing density. Thus the temperature gradient (2.7) becomes negligible at densities much above 10^{10} $g\,cm^{-3}$. This allows a natural division of the star into two regions: an 'isothermal' core and an outer envelope. By 'isothermal' one means that there is no thermal energy flux. As a consequence of the gravitational redshift this implies that Te^{ϕ} = constant. It should be noted that the outer envelope contains a negligible frac-

tion of the star's mass and heat.

The rate of loss of internal energy is found by integrating eqns. (2.4) and (2.6) through the isothermal core:

$$L(R_c)e^{2\phi_c} = -\int_{r=0}^{R_c} ne^{\phi} T \frac{ds}{dt} \frac{4\pi r^2 dr}{(1-2Gm/rc^2)^{1/2}} \qquad (2.10)$$

$$L_\nu(R_c)e^{2\phi_c} = \int_{r=0}^{R_c} nq_\nu r^{2\phi} \frac{4\pi r^2 dr}{(1-2Gm/rc^2)^{1/2}} . \qquad (2.11)$$

Here $\phi_c = \phi(R_c)$ is the gravitational potential at the core-envelope boundary, $r = R_c$. The entropy derivative in eqn. (2.10) may be written in terms of the specific heat:

$$T \frac{ds}{dt} = T \frac{ds}{dT} \frac{dT}{dt} = C_v \frac{dT}{dt} . \qquad (2.13)$$

Define a new temperature parameter $T' = Te^{\phi}$. Then

$$\frac{dT'}{dt} = e^{\phi} \frac{dT}{dt} + T \frac{de^{\phi}}{dt}$$

$$= e^{\phi} \frac{dT}{dt}$$

since the structure of the star does not change with time.

As already seen, T' is independent of radius at all times (in the core). It follows that $\frac{dT'}{dt}$ is also independent of radius. Therefore eqns. (2.10) and (2.11) may be rewritten as:

$$L(R_c)e^{2\phi_c} = \int_{r=0}^{R_c} nC_v \frac{dT'}{dt} \frac{4\pi r^2 dr}{(1-2Gm/rc^2)^{1/2}}$$

$$= -\frac{dT'}{dt} \int_{r=0}^{R_c} nC_v \, dV_p \qquad (2.14)$$

and

$$L_\nu(R_c)e^{2\phi_c} = \int_{r=0}^{R_c} nq_\nu e^{2\phi} \, dV_p \qquad (2.15)$$

where dV_p is the differential for the proper volume.

Our goal is to determine the surface temperature of a neutron star as a function of time. Rewriting eqn. (2.14) gives the following equation for the rate of change of the core temperature:

$$-\frac{dT'}{dt} = \frac{L(R_c)e^{2\phi_c}}{\int nC_v dV_p}$$

$$= \frac{L_\nu(R_c)e^{2\phi_c} + L_\gamma(R_c)e^{2\phi_c}}{\int nC_v dV_p} \qquad (2.16)$$

Each of the three terms on the right side of eqn. (2.16) must be evaluated as a function of T'. The specific heat and neutrino luminosity depend simply on the density, temperature and gravitational potential; and the relevant terms are evaluated in chapters four and five. The photon

luminosity depends on the effective surface temperature T_s.

Thus, to solve for the cooling curve, the relationship between the core and surface temperatures must be established. We turn to the determination of this relationship in the next chapter.

CHAPTER III

THE CORE-SURFACE TEMPERATURE RATIO

To solve for the cooling curve, the surface temperature must be found as a function of core temperature. This is accomplished by integrating the temperature gradient (2.7) throughout the outer envelope. However, as eqn. (2.7) is coupled to the other equations of stellar structure (2.1)-(2.6), the whole set should be solved simultaneously. This can be much simplified by using certain approximations valid in the outer envelope.

III.1 Equations for the Outer Envelope

a) Mass and Pressure

The outer envelope contains a negligible fraction (about 10^{-6}) of the star's mass. Therefore $m(r) \approx M$, the total mass of the star.

The pressure at a given point is just the weight per unit area of the matter above. Therefore, with Δm being the mass of the outer envelope,

$$\frac{4\pi r^2 P}{c^2} = \frac{GM\Delta m}{rc^2} << M \qquad (3.1)$$

since $\Delta m << M$ and $\frac{GM}{rc^2} < 1$. Thus, in eqns. (2.2) and (2.3), we can set

$$m + \frac{4\pi r^3 P}{c^2} = M. \qquad (3.2)$$

b) Gravitational Potential

Outside a spherically symmetric star the potential is given by the exterior Schwarzschild solution

$$e^{\phi} = (1-2GM/rc^2)^{1/2} . \qquad (3.3)$$

This is valid throughout the outer envelope to the extent that $m(r) \approx M$.

c) Luminosity

It follows from eqns. (2.4) and (2.6) that in the absence of local energy sources then $Le^{2\phi}$ and $L_\nu e^{2\phi}$ are independent of radius. Together with eqn. (2.5) this implies that

$$L_\gamma e^{2\phi} = \text{constant}, \qquad (3.4)$$

valid as there are negligible energy sources in the outer envelope. At the surface, the photon luminosity defines an effective blackbody temperature T_s:

$$L_\gamma(R) = 4\pi R^2 \sigma T_s^4 . \qquad (3.5)$$

Thus, for the photon luminosity in eqn. (2.16) we have

$$L_\gamma(R_c)e^{2\phi_c} = L_\gamma(R)e^{2\phi(R)} = 4\pi R^2 g T_s^4 e^{2\phi(R)} . \qquad (3.6)$$

d) Temperature Gradient

It is simplest to take the pressure as the independent variable.

$$\frac{dT^4}{dp} = 4T^3 \frac{dT}{dr}\frac{dr}{dp}$$

$$= \frac{3\kappa R^2 T_s^4 e^{\phi}}{4GM(1 + \frac{P}{\rho c^2})} + \frac{4T^4}{\rho c^2 + P} \qquad (3.7)$$

as follows from eqns. (2.2), (2.7) and (3.3). The second term on the right hand side is a relativistic effect arising from the gravitational potential.

Equation (3.7) is to be integrated from the photosphere (defined below) inward to a density of 2×10^{10} g-cm^3, above which the star is isothermal (Te^{ϕ} = constant). The surface temperature T_s is taken to be a free parameter. To do the integration two functions are needed: $\rho(P,T)$ and $\kappa(\rho,T)$. These functions are discussed in the remainder of the chapter.

To check the assumptions that the mass and thickness of the outer envelope are small, equations (2.1) and (2.2) are integrated as well.

The integrations are done numerically using the Runge-Kutta method, which is accurate to fourth order in the step size. The step size is chosen so that neither the pressure nor the temperature change by more than ten per-cent per

step.

The boundary condition on the pressure at the surface (photosphere) is given by (Thorne 1967)

$$K_R(R)P(R) = \frac{2GM}{3R^2 e^{\varphi(R)}}$$

where K_R is the radiative opacity. This corresponds to an optical depth of 2/3.

III.2 Equation of State

a) Composition

It is commonly supposed that the matter in a neutron star will be in the most energetically favourable state, as a result of the tremendous thermonuclear activity accompanying the formation of the star. At densities below 10^7 g-cm^{-3}, the most stable state is ^{56}Fe nuclei in an electron sea. At higher densities, more neutron-rich nuclei are favoured because of the large Fermi energy of the electrons. The results of Baym, Pethick and Sutherland (1971) for the composition in the outer envelope are generally accepted and are used here.

Two points should be noted here. If the star accretes matter, there may form a blanket of hydrogen or helium at the surface, as is suggested in the case of X-ray bursters. Secondly, the surface layers of a neutron star may be significantly affected by a strong magnetic field (Ruderman,

1971, 1974), such as are found in pulsars. These possibilities are not considered further at the present.

The composition enters the equation of state in two ways: in the number of nucleons per free electron, μ_e; and in the mass of the ions, m_i (in proton masses).

The number of free electrons per nucleon is

$$\frac{1}{\mu_e} = \frac{Z}{A} f \qquad (3.9)$$

where f is the fractional ionization. The following approximation is used for f (CGS units)

$$f = \max\{0.303 \log (0.2\rho), 0.926 \log (1.357\times10^{-18}T^4\rho^{-0.313})\} \qquad (3.10)$$

with cutoffs $0 \leq f \leq 1$. This expression is adequate for ^{56}Fe.

b) Contributions to the Pressure

The pressure in the outer envelope comes from three sources: the electrons, the ions, and the radiation. These terms can be written as

$$P = P_e + \frac{\rho kT}{m_i} + \frac{a}{3} T^4 . \qquad (3.11)$$

The pressure and temperature are known, and the density must be solved for. As the electron pressure P_e is density dependent, the density must be solved for iteratively.

The ion pressure is much less than the electron pressure (except under conditions where f is very small). If a reasonable estimate of the density is used to evaluate the ion pressure, the electron pressure may be solved for from eqn. (3.11) with small error. This value for the electron pressure will yield a density that can be put back into eqn. (3.11) to check for self-consistenty.

c) The Density as a Function of Electron Pressure

The following definitions are useful.

$$\alpha = -\frac{\mu}{kT} \quad , \qquad \mu = \text{chemical potential} \tag{3.12}$$

$$\beta = \frac{kT}{m_e c^2} \quad , \qquad m_e = \text{electron mass} \ . \tag{3.13}$$

As shown in Appendix A, the electron pressure may be written as

$$P_e = \frac{8\pi kT}{3h^3} (2m_e kT)^{3/2} G(\alpha,\beta) \tag{3.14}$$

with

$$G(\alpha,\beta) = \int_0^\infty \frac{x^{3/2}(1 + \frac{1}{2}\beta x)^{3/2} dx}{1 + e^{\alpha+x}} \ ; \tag{3.15}$$

and the density may be written as

$$\rho = \mu_e m_p \frac{4\pi}{h^3} (2m_e kT)^{3/2} H(\alpha,\beta) \tag{3.16}$$

with

$$H(\alpha,\beta) = \int_0^\infty \frac{x^{1/2}(1+\beta x)\left(1+\frac{1}{2}\beta x\right)^{1/2} dx}{1+e^{\alpha+x}} . \qquad (3.17)$$

Equation (3.14) must be solved for α. This could be done by evaluating the integral (3.15) numerically at an array of points in the (α,β) plane and interpolating. However, to achieve the desired accuracy this would require a prohibitively large number of integrals.

The problem is simplified by dividing the $(\alpha-\beta)$ plane into four regions. In three of these regions $G(\alpha,\beta)$ and $H(\alpha,\beta)$ can be expanded in series, eliminating the need to do the integrals.

The four regions are:

i) Non-degenerate region ($\alpha \gg 0$)

The boundary is taken to be $G(\alpha,\beta) < 0.024+0.07\ \beta$, (or $\alpha < -8$). $G(\alpha,\beta)$ can be expanded in a power series in $e^{-\alpha}$.

$$G(\alpha,\beta) = \sum_j e^{-j\alpha}(-1)^{j+1} \frac{3}{2^{3/2} j^{5/2}} x^{1/2} e^{x} K_2(x)$$

$$= c_1(\beta)e^{-\alpha} + c_2(\beta)e^{-2\alpha} + c_3(\beta)e^{-3\alpha} + \cdots \qquad (3.18)$$

Here $x = j/\beta$ and $K_2(x)$ is a modified Bessel function. Solving for $e^{-\alpha}$,

$$e^{-\alpha} = \frac{G(\alpha,\beta)}{c_1(\beta)} - \frac{c_2(\beta)}{c_1^3(\beta)} G^2(\alpha,\beta) + \left[\frac{2c_2^2(\beta)}{c_1^5(\beta)} - \frac{c_3(\beta)}{c_1^4(\beta)}\right] G^3(\alpha,\beta) \cdots . \qquad (3.19)$$

$H(\alpha,\beta)$ can also be expanded in a power series. The result is

$$H(\alpha,\beta) = \frac{2}{3} c_1(\beta)e^{-\alpha} + \frac{4}{3} c_2(\beta)e^{-2\alpha} + \frac{6}{3} c_3(\beta)e^{-3\alpha} + \ldots \quad (3.20)$$

which is evaluated using eqn. (3.19).

ii) Strongly degenerate region ($\alpha \ll 0$)

The boundary is taken to be $G(\alpha,\beta) > 80+550\ \beta$, (or $\alpha > 4$). The integrals $G(\alpha,\beta)$ and $H(\alpha,\beta)$ can be expanded using Sommerfeld's lemma (see for example, Chandrasekhar 1939). After some lengthy algebra one finds:

$$G(\alpha,\beta) = \frac{1}{16\sqrt{2}\beta^{5/2}}\{(2x-3+4\pi\beta^2)(x^2+x)^{1/2}+3\ln(x^{1/2}+(1+x)^{1/2}) + \frac{7\pi^4\beta^4}{15}(2x-1)\left(\frac{x+1}{x^3}\right)^{1/2}\} \quad (3.21)$$

$$H(\alpha,\beta) = \frac{x^{3/2}}{3\sqrt{2}\ \beta^{3/2}}\left\{1 + \frac{\pi^2\beta^2}{2}\frac{(2x+1)}{x^2} + \frac{7\pi^4\beta^4}{40x^4}\right\} . \quad (3.22)$$

Here $x = \alpha^2\beta^2 + |2\alpha\beta|$.

The right hand side of eqn. (3.21) is a monotonic function of x at fixed β, so the equation can be solved for x by using a simple root finding procedure. $H(\alpha,\beta)$ can then be evaluated.

iii) Intermediate degeneracy, small β region ($\beta < 0.01$)

Expanding eqns. (3.15) and (3.17) in powers of β one gets:

$$G(\alpha,\beta) = \int_0^\infty \frac{x^{3/2}dx}{1+e^{\alpha+x}} + \frac{3\beta}{4}\int_0^\infty \frac{x^{5/2}dx}{1+e^{\alpha+x}} + \frac{3\beta^2}{16}\int_0^\infty \frac{x^{7/2}dx}{1+e^{\alpha+x}} + \ldots \quad (3.23)$$

$$H(\alpha,\beta) = \int_0^\infty \frac{x^{1/2}dx}{1+e^{\alpha+x}} + \frac{5\beta}{4}\int_0^\infty \frac{x^{3/2}dx}{1+e^{\alpha+x}} + \frac{7\beta^2}{32}\int_0^\infty \frac{x^{5/2}dx}{1+e^{\alpha+x}} + \ldots \quad (3.24)$$

The above integrals are evaluated numerically for $-8 \leq \alpha \leq 4$, in steps of $\alpha = 0.2$. Eqn. (3.23) is solved for α using a quadratic interpolation from the nearest three points. Then the integrals in eqn. (3.24) are similarly evaluated by interpolation.

iv) Intermediate degeneracy region, $\beta > 0.01$

The integrals for $G(\alpha,\beta)$ and $H(\alpha,\beta)$ are evaluated numerically at an array of points in the $(\alpha-\beta)$ plane. A two-dimensional interpolation is used to find α, and then $H(\alpha,\beta)$ may also be evaluated by interpolation.

This method is straightforward, but is cumbersome because of the large number of integrals to evaluate. To achieve the desired accuracy within the restricted region $-8 < \alpha < 4$, $\beta > 0.1$, a total of three thousand integrals are used. This prevents the method from being used for all α and β.

Once $H(\alpha,\beta)$ is evaluated, the density resulting from eqn. (3.16) may be tested for self-consistency. If the two sides of eqn. (3.11) differ by more than 0.01% the process is repeated. This method converges quickly to the correct density.

II.3 Opacity

There are three possible means of energy transport in a star: radiative, conductive, and convective. Neutron stars are found not to have convective regions. Conduction by electrons is the most important method of energy transport, except in the non-degenerate outermost layer, where radiative transport dominates.

Opacity is a measure of 'resistance' to energy transport. An opacity to thermal conduction (κ_c), and an opacity to radiation (κ_R), may be defined. The total opacity is then given by

$$\frac{1}{\kappa} = \frac{1}{\kappa_R} + \frac{1}{\kappa_c} \qquad (3.25)$$

which is dominated by the smaller of κ_R and κ_c.

For densities less than 10^4 g-cm^{-3} both κ_R and κ_c have been provided for pure ^{56}Fe by the Los Alamos library (Huebner et al. 1977). At higher densities the results of Flowers and Itoh (1976) have been used. Some extrapolation and interpolation has had to be done to obtain the necessary

values. The effects of a magnetic field on the opacity are discussed at the end of this chapter.

Radiative Opacity

Tables of the radiative opacity κ_R in the low-density region were kindly provided by the Los Alamos group. At high temperatures these tables had to be extrapolated to higher densities where the conductive opacity becomes dominant (see Figure 3.1). Although this extrapolation becomes suspect for $T >> 10^8$K, this is unimportant for two reasons. Firstly, for outer layers at these temperatures the neutrino emission from the core completely controls the cooling rate. Secondly, the star will remain this hot only for the first year or so after its formation.

Conductive Opacity

The conductive opacity κ_c is related to the thermal conductivity λ_c by

$$\kappa_c = \frac{16\sigma T^3}{3\rho\lambda_c} = 3.024\times10^{-4}\ \frac{T^3}{\rho\lambda_c}\ . \qquad (3.26)$$

Flowers and Itoh (1976) present tabulated calculations of the thermal conductivity in the region $\rho > 10^4$ g-cm^{-3}, $T > 10^6$K. Their calculations include contributions from electron-electron scattering, electron-phonon and electron-impurity scattering (below the lattice melting temperature), and electron-ion scattering (above the lattice melting tem-

perature). To make use of their results one must specify a lattice melting temperature, which (following them), we take to be given by

$$T_m = 3.7\times10^3 \rho^{1/3} (\frac{2Z}{A}) Z^{5/3} \qquad (3.27)$$

where Z,A are the charge and mass numbers for the lattice ions. One must also specify a parameter for the charge fluctuations due to impurities $x_i<(\Delta Z)^2>$, with x_i being the fractional concentration of impurities. A value of $x_i<(\Delta z)^2>$ = 1 has been used throughout. The electron-electron scattering term does not appear in previous calculations of the thermal conductivity (eg. Hubbard and Lampe, 1969), but its significance is diminished since the radiative opacity dominates when the electron-electron scattering is largest.

The Los Alamos group have also provided conductive opacities at low densities. Although these never dominate the radiative opacity they are useful in helping to extrapolate the Flowers and Itoh results, especially at low temperatures.

Figure (3.1) summarizes the above points, and also illustrates the temperature-density profiles of a typical neutron star at three characteristic surface temperatures. It can be seen that the tabulated opacities fairly well cover the regions of interest.

Figure 3-1

Envelope profiles in the temperature-density plane for a 1.25 $M_\odot$ neutron star, stiff equation of state (PPS), and zero magnetic field. The solid curves are for surface temperatures of $10^{5.5}$, $10^{6.0}$, and $10^{6.5}$ K. The plane is divided into several regions: in the upper left (stippled) region the radiative and conductive opacities from Los Alamos (Huebner et al. 1977) are used, and in the upper right region the conductivity calculations of Flowers and Itoh (1976) are used; elsewhere interpolation and extrapolation are used. The dashed lines roughly divide the plane according to degeneracy (non-degenerate above) and according to mode of energy transport (conductive below).

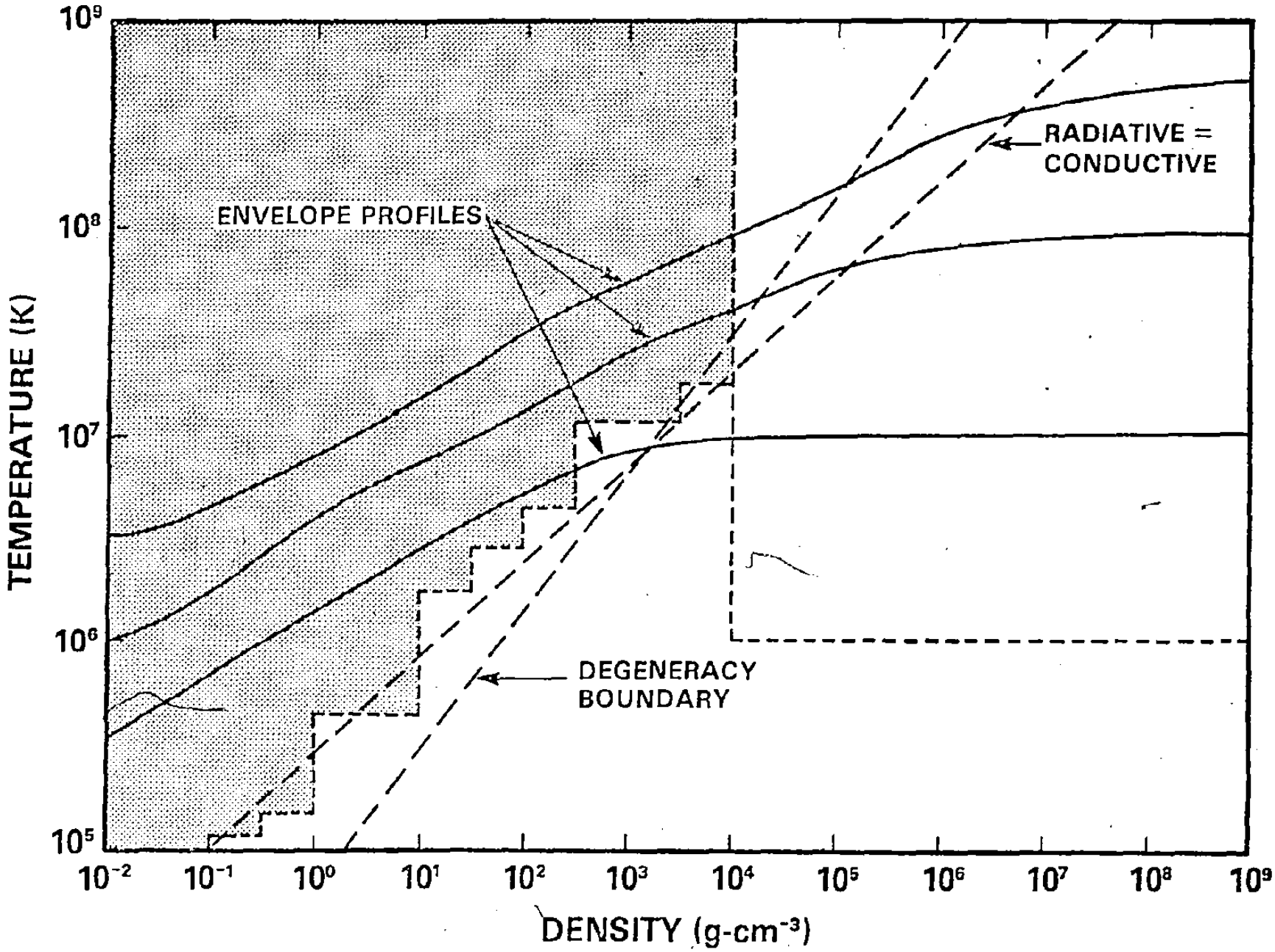
ENVELOPE PROFILES
RADIATIVE = CONDUCTIVE
DEGENERACY BOUNDARY
TEMPERATURE (K)
DENSITY (g-cm⁻³)
10⁹
10⁸
10⁷
10⁶
10⁵
10⁻²
10⁻¹
10⁰
10¹
10²
10³
10⁴
10⁵
10⁶
10⁷
10⁸
10⁹

Figure 3-1

III.4 Magnetic Fields

Some neutron stars may have very strong magnetic fields (e.g. $B \approx 10^{12}$ G for a pulsar). A magnetic field of this size does not appreciably alter the structure of the star, except in the outermost layers where the pressure is small. It has been suggested (Ruderman 1971,1974) that the surface layer of a magnetized star may be a highly anisotropic 'magnetic metal', terminating abruptly at a density near 10^4 g-cm^{-3}; however the properties of such exotic matter have not been reliably calculated to date. Therefore in the present work we take no account of any magnetic modifications to the low density equation of state. We do consider the modification of the radiative and conductive opacities by the field: these will change (reduce) the core-surface temperature ratio.

Radiative Opacity

It has been shown (Lodenquai et al. 1974) that the radiative opacity in a strong magnetic field is approximately related to the zero-field opacity by

$$\kappa_R(\omega,B) = \frac{\omega^2}{\omega_c^2}\,\kappa_R(\omega,B=0) \quad , \quad \omega << \omega_c \qquad (3.28)$$

where $\omega_c = \frac{eB}{m_e c}$ is the cyclotron frequency and ω is the radiation frequency.

For temperatures much greater than 10^7K the typical

photon frequency $\omega \sim \frac{kT}{\hbar}$ is comparable to the cyclotron frequency for magnetic fields $\sim 10^{12}$ G. Therefore, the following expression (derived in Appendix B) is used instead.

$$\kappa_R(\omega,B) = \frac{\omega^2}{\omega^2+\omega_c^2}\,\kappa_R(\omega,B=0) \quad . \tag{3.29}$$

This has the correct limits for both large and small magnetic fields.

To obtain a frequency independent opacity the Rosseland mean is used

$$\frac{1}{\kappa_R} = \int_0^\infty \frac{1}{\kappa_R(\omega)}\,\frac{dB}{dT}\,d\omega \Bigg/ \int_0^\infty \frac{dB}{dT}\,d\omega \quad . \tag{3.30}$$

Here $B(\omega)$ is the Planck blackbody distribution.

To evaluate the Rosseland mean the frequency dependence of $\kappa(\omega,B=0)$ is needed. For the opacity due to free-free transitions $\kappa_{ff} \propto \omega^{-7/2}$. However, at low densities and at high temperatures (the regions where electron conduction is least effective) the radiative opacity is dominated by Thompson scattering, which is frequency independent.

The result in this case is then

$$\kappa_R(B) = \frac{\kappa_R(B=0)}{1 + 0.23\ B_{12}^2/T_8^2} \tag{3.31}$$

where B_{12} and T_8 are the magnetic field in units of 10^{12} G and the temperature in 10^8 K, respectively.

Conductive Opacity

The conductive opacity in a magnetic field is expressed as

$$\kappa_c(B) = a_c \kappa_c(B=0) \quad , \quad a_c \leq 1 \; . \tag{3.32}$$

The factor a_c is a function of the density, temperature, and magnetic field intensity. Graphs of $a_c(\rho)$ for various magnetic fields are given by Tsuruta (1974) based on earlier calculations by Canuto and Chiu (1969), and are used here. The temperature dependence drops out if the electrons are degenerate, as they are when conduction dominates the energy transport.

The total opacity is given by the standard relation $\kappa^{-1}(B) = \kappa_R^{-1}(B) + \kappa_c^{-1}(B)$, identical in form to the case with zero magnetic field.

Apart from the only approximate expressions used here for the opacity in a magnetic field, there are several other important effects which are being neglected. The additional anisotropy (polarization dependence in the case of radiation) of energy transport due to the field is being crudely averaged over. In reality the thermal radiation from the star will not be spherically symmetric and, if the neutron star should also rotate, this could appear as a "pulsation". Further-

more, the strength of the magnetic field will vary over the surface of the star (by a factor of two in the simplest dipole case). Thus the single magnetic field parameter used in the opacity is somewhat ill-defined and is intended to represent an average effect.

Figure 3-2

Relationship between temperature at the core/envelope boundary and temperature at the surface, for neutron stars of 1.25 $M_\odot$, with the soft BPS EOS (——— B = 0; ····· B = 10^{12} G) and with the stiff PPS EOS (----- V = 0; -·-·-; B = 10^{12} G).

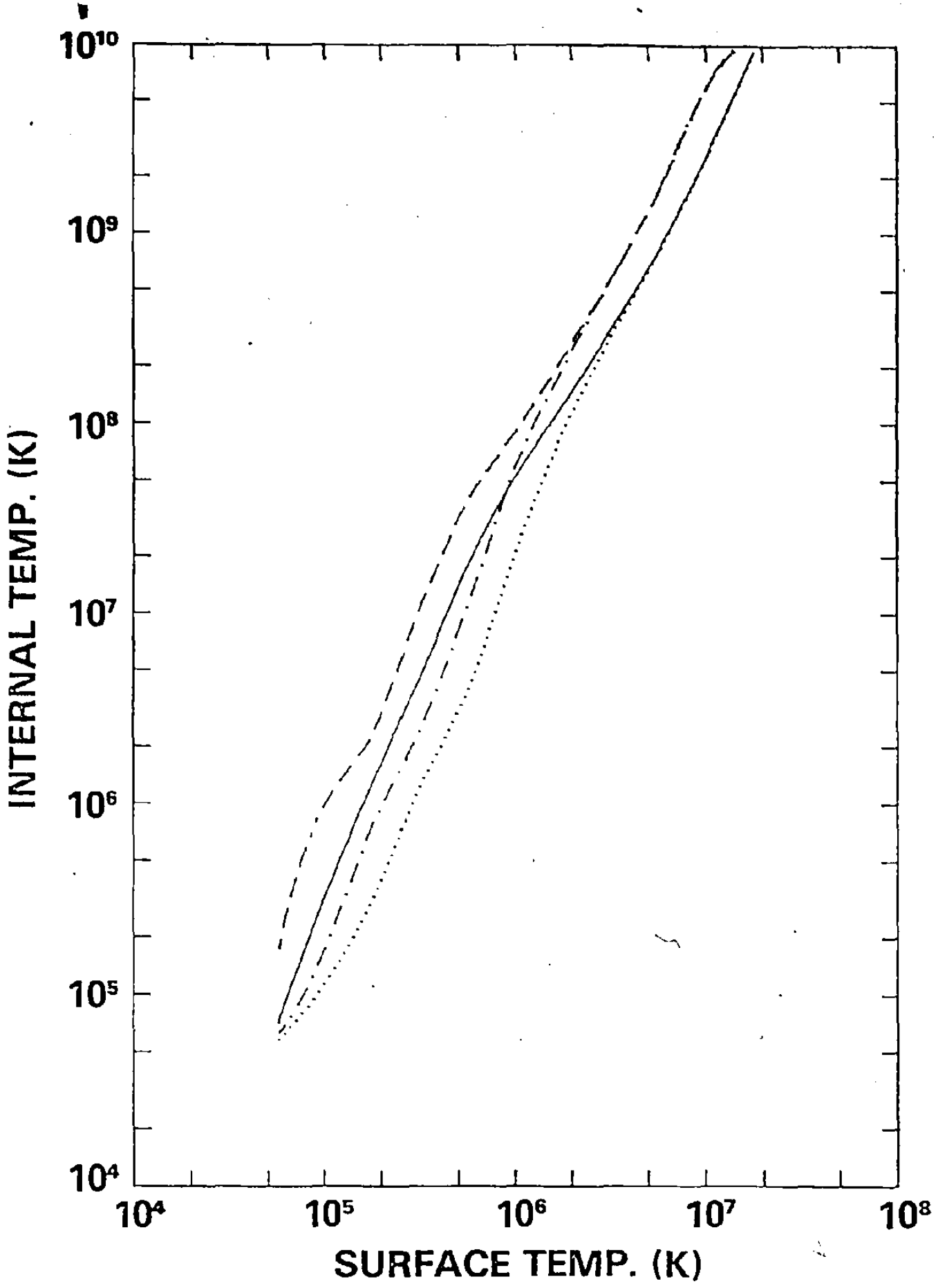
INTERNAL TEMP. (K)
10^{10}
10^{9}
10^{8}
10^{7}
10^{6}
10^{5}
10^{4}
10^{4}
10^{5}
10^{6}
10^{7}
10^{8}
SURFACE TEMP. (K)

Figure 3-2

CHAPTER IV

SPECIFIC HEAT

To solve equation (2.16) for the cooling rate it is necessary to know C_v, the specific heat per particle, throughout the star. Contributions to the specific heat come from the neutrons, protons, electrons, crustal ions, muons and hyperons. The hyperons are present only at the highest densities, and are omitted hereafter since the parameters are not well known. Apart from the ions, the particles are all degenerate Fermi gases.

To determine the heat content of the core, the Fermi momenta and energies are needed.

Fermi Momenta

For spin $\frac{1}{2}$ fermions the Fermi momentum is related to the number density of particles of type (i) by

$$\frac{k_F^3(i)}{3\pi^2} = n(i) \tag{4.1}$$

$$\therefore \quad p_F(i) = \hbar k_F(i) = \hbar[3\pi^2 n(i)]^{1/3} . \tag{4.2}$$

For the neutrons, $n(N) = \frac{\rho_N}{m_N}$, and therefore for $\rho_N \approx \rho$

$$p_F(N) \approx 336.5 \left(\frac{\rho}{\rho_0}\right)^{1/3} \frac{MeV}{c} \tag{4.3}$$

where $\rho_0 = 2.8\times10^{14}$ g-cm^{-3} (nuclear matter density).
For the free protons, electrons and muons, by charge neutrality (in the absence of ions)

$$n(p) = n(e) + n(\mu) \tag{4.4}$$

$$\therefore \quad p_F^3(p) = p_F^3(e) + p_F^3(\mu) \tag{4.5}$$

Fermi Energies

The electrons are extremely relativistic and have Fermi energy $\varepsilon_F(e) = cp_F(e)$. In beta equilibrium the electrons and muons must have equal energies

$$cp_F(e) = (m_\mu^2c^4 + c^2p_F^2(\mu))^{1/2} \quad , \quad \text{for } cp_F(e) > m_\mu c^2 \ . \tag{4.6}$$

(The thermal energies of the particles are negligible since $kT < 1$ MeV $<< \varepsilon_F$.)

For the protons and neutrons it is useful to introduce the effective masses m_p^* and m_N^*, defined in the non-relativistic limit by

$$m_i^* = p_F(i)\,\frac{dp_F(i)}{d\varepsilon_F(i)} \ . \tag{4.7}$$

If m_i^* is independent of the Fermi momentum (or density) then eqn. (4.7) integrates to give

$$\varepsilon_F(i) = \frac{p_F^2(i)}{2m_i^*} \ . \tag{4.8}$$

The non-relativistic limit is valid for the protons. The neutrons become relativistic at the very highest densities

($\rho > 3\times10^{15}$ g-cm^{-3}), but the non-relativistic limit is used for simplicity.

For the protons, $\frac{m_p^*}{m_p}$ is taken to be one at all densities, so eqn. (4.8) holds. For the neutrons, the effective mass of Takatsuka (1972) is used. This is approximated by

$$\frac{m_N^*}{m_N} = \min\left(1, 0.885\left(\frac{\rho}{\rho_0}\right)^{-0.032}, 0.815\left(\frac{\rho}{\rho_0}\right)^{-0.135}\right) \quad (4.9)$$

which has a weak density dependence. Integrating eqn. (4.7) with this effective mass yields

$$\varepsilon_F(N) = \frac{p_F^2(N)}{2m_N^* f} \quad (4.10)$$

where

$$f = 1.14 + 0.04\left(\frac{\rho}{\rho_0}\right)^{0.4} . \quad (4.11)$$

(There is considerable uncertainty about the values of m_p^* and m_N^*. Takatsuka's value for m_N^* is used since his superfluidity parameters (dependent on m_N^*) are later used.)

The neutrons, protons and electrons are in β-equilibrium

$$cp_F(e) + m_p c^2 + \frac{p_F^2(p)}{2m_p^*} = m_N c^2 + \frac{p_f^2(N)}{2m_N^* f} . \quad (4.12)$$

Since $m_N c^2 - m_p c^2 \approx 1$ MeV $<<$ other terms, and in the absence of muons $p_F(p) = p_F(e)$, we have

$$cp_F(e) + \frac{p_F^2(e)}{2m_p^*} \approx \frac{p_F^2(N)}{2m_N^* f} \quad (4.13)$$

which is a quadratic with solution

$$cp_F(e) = m_p^* c^2 \left[\left(1 + \frac{p_F^2(N)}{m_p^* m_N^* f c^2} \right)^{1/2} - 1 \right] \qquad (4.14)$$

which is evaluated using eqn. (4.3).

Now $p_F(\mu)$ is evaluated using eqn. (4.6) and $n(p)$ found from eqns. (4.4) and (4.5). Since the density appearing in eqn. (4.3) should really be ρ_N, a first-order correction is made by using $n(p)$ and

$$p_F(N) = 336.5 \left(\frac{\rho - n(p) m_p}{\rho_0} \right)^{1/3} \frac{MeV}{c} \qquad (4.15)$$

in eqn. (4.14), and repeating the calculation.

IV.1 Specific Heat of Fermions

The specific heat per particle of a degenerate ($kT << \varepsilon_F$) Fermi gas is (Ziman 1960)

$$C_v = \frac{\pi^2}{3} k^2 T \frac{N(\varepsilon_F)}{n} . \qquad (4.16)$$

$N(\varepsilon_F) = \frac{dn}{d\varepsilon_F}$ is the density of states at the Fermi surface. There are two cases:

i) Non-relativistic particles (neutrons and protons)

Equations (4.7) and (4.2) yield

$$N(\varepsilon_F) = \frac{dn}{dp_F} \frac{dp_F}{d\varepsilon_F} = \frac{3nm^*}{p_F^2} \qquad (4.17)$$

and thus the specific heat per unit volume is

$$n(i)C_v(i) = n(i)\ \frac{\pi^2}{3}\ k^2T\ \frac{3m_i^*}{p_F^2(i)} = 1.63\times10^{11}\left(\frac{m_i^*}{m_i}\right)\left(\frac{\rho_i}{\rho_0}\right)^{1/3} T \quad \text{erg-cm}^{-3}\text{-K}^{-1} \qquad (4.18)$$

ii) Relativistic particles (electrons and muons)

$$\varepsilon_F = (m^2c^4 + c^2p_F^2)^{1/2} - mc^2 \qquad (4.19)$$

$$\frac{d\varepsilon_F}{dp_F} = (m^2c^4 + c^2p_F^2)^{-1/2} c^2p_F \qquad (4.20)$$

$$N(\varepsilon_F) = \frac{dn}{dp_F}\frac{dp_F}{d\varepsilon_F} = \frac{3n(m^2c^4+c^2p_F^2)^{1/2}}{c^2p_F^2} \qquad (4.21)$$

$$n(i)C_v(i) = n(i)\pi^2k^2T\ \frac{[m_i^2c^4+c^2p_F^2(i)]^{1/2}}{c^2p_F^2(i)} . \qquad (4.22)$$

For electrons $m_e^2c^4 << c^2p_F^2(e)$

$$n(e)C_v(e) = \frac{k_F^3(e)}{3\pi^2}\ \frac{\pi^2k^2T}{cp_F(e)}$$

$$= \frac{c^2p_F^2(e)}{3c^3\hbar^3}\ k^2T. \qquad (4.23)$$

For muons, using eqn. (4.6)

$$n(\mu)C_v(\mu) = \frac{p_F^3(\mu)}{3\pi^2\hbar^3}\ \pi^2k^2T\ \frac{cp_F(e)}{c^2p_F^2(\mu)}$$

$$= \begin{cases} \dfrac{k^2T}{3c^3\hbar^3}\ cp_F(e)\,(c^2p_F^2-m_\mu^2c^4)^{1/2}, & cp_F(e) > m_\mu c^2 \\ 0, & cp_F(e) \le m_\mu c^2 \end{cases} \qquad (4.24)$$

At densities below 2×10^{14} g-cm^3 there are no free protons, but instead there are crustal ions. The number densities of ions, neutrons and electrons are calculated from the results of Negele and Vautherin (1973). The following parametrizations are made:

$$n_e = \max[5\times10^{36}(\frac{\rho}{\rho_0})^{1.04}, 1.29\times10^{36}(\frac{\rho}{\rho_0})^{0.48}] \quad (4.25)$$

$$n_{ion} = \max[4\times10^{34}(\frac{\rho}{\rho_0})^{0.61}, 1.38\times10^{34}(\frac{\rho}{\rho_0})^{0.33}] \quad (4.26)$$

$$\frac{\rho_N}{\rho} = \min[0.816\ \log\rho+2.414, 0.15\ \log\rho+1.055, 0.05\ \log\rho+0.947] \quad (4.27)$$

with the condition $\rho_N \geq 0$.

In the crust ($\rho < 2\times10^{14}$ g-cm^{-3}), the neutron and electron specific heats are given by eqns. (4.18) and (4.23), with the densities (4.27) and (4.25), respectively.

According to Flowers and Itoh (1976) the ions form a lattice with a melting temperature $T_m >> 10^9$K (except in the outer envelope). Therefore, the ions are taken to be a solid with Debye specific heat

$$n(\text{ions})C_v(\text{ions}) = 3k\, n(\text{ions})\mathcal{D}(\theta_D/T) \quad (4.28)$$

θ_D is the Debye temperature $= \min[1.5\times10^{10}(\frac{\rho}{\rho_0})^{0.38}, 5\times10^9]$. $\mathcal{D}(x)$ is the Debye function, which has limits

$$\mathcal{D}(x) \to 1 \ , \ x \text{ small}$$

$$\mathcal{D}(x) = \frac{4\pi^4}{5x^3} \ , \ x \text{ large} \quad (T^3 \text{ law}) \ .$$

IV.2 Superfluid Specific Heat

At certain densities and temperatures the protons and neutrons may be in superfluid states. If so, then the specific heat is modified from the previous result (4.18) by a factor Y_s. Maxwell (1979) gives a graph of Y_s versus T/T_c, where T_c is the superfluid transition temperature. This graph is fitted by

$$Y_s = 3.47\ (\frac{T}{T_c} - 0.2)^{1.6}\ ,\quad 0.2 \leq \frac{T}{T_c} < 1$$

$$= 0\ ,\quad T < 0.2\ T_c$$

$$= 1\ ,\quad T > T_c\ . \qquad (4.29)$$

The transition temperature T_c is a function of the Fermi energy. The results of Takatsuka (1972) are used for $T_c(\varepsilon_F)$.

For nucleon Fermi energies between 1 MeV and 40 MeV the possibility of s-wave superfluidity exists, and for Fermi energies from 50 MeV to 120 MeV the possibility of p-wave superfluidity exists.

The protons are all in the s-wave region ($\varepsilon_F \simeq$ 1-40 MeV). The neutrons will form two bands of superfluid regions (s-wave and p-wave), with the remaining neutrons in the normal state.

If the neutrons are in the normal state, they contribute most of the specific heat of the star. If the neutrons

are superfluid, the protons should be as well, and the electron may become the major source of specific heat. The crustal ions may be important under certain conditions.

IV.3 Zoning and Equation of State

To evaluate the temperature derivative (2.16) the specific heat (and neutrino luminosity) must be integrated throughout the star. Since the integrands have complicated density dependencies, it is expedient to divide the star into concentric shells of constant density, temperature, and gravitational potential; and to replace the integrals with summations.

$$\int_{r=0}^{R_c} nq_\nu e^{2\phi(r)} dV_p \rightarrow \sum_j V_p(j) e^{2\phi_j} (nq_\nu)_j \qquad (4.30)$$

$$\int_{r=0}^{R_c} nC_v dV_p \rightarrow \sum_j (nC_v)_j V_p(j) \quad . \qquad (4.31)$$

To find the proper volume, average density and gravitational potential of each zone, the equations of stellar structure (2.1), (2.2) and (2.3) are integrated along with a zero temperature equation of state.

There is some doubt as to what equation of state is valid at neutron star densities. To test the sensitivity of the results to the equation of state, two (possibly extreme) equations of state are used. These are: (A) the equation of

state of Baym, Pethick and Sutherland (1971). hereafter referred to as BPS; and (B) the TI equation of state of Pandharipande, Pines and Smith (1976), hereafter referred to as PPS. The BPS equation of state is much softer than that of PPS, allowing higher central densities and smaller radii. For the same mass, a star with the stiffer PPS equation of state has a larger radius and lower central density, thus a larger crust and larger superfluid regions than the corresponding BPS model.

The stars are divided into forty zones, chosen so that fifteen zones have densities between $\rho = 5\times10^{9}$ and $\rho = 5\times10^{-13}$ g-cm^{-3}, with a further twenty-five zones interior to these. The density ratios between successive zones is constant in each of the two regions.

The expression for the neutrino emissivity is determined in the next section.

Figure 4-1

Specific heat contributions for neutron star matter at density $\rho = 10^{14}$ g-cm^3: normal neutrons (-----), superfluid neutrons Takatsuka (1972, -·-·-·), electrons (———), and ion lattice (·····). At this density there are no free protons. The soft and stiff EOS's are identical at densities below that of nuclear matter (2.8×10^{14} g-cm^{-3}).

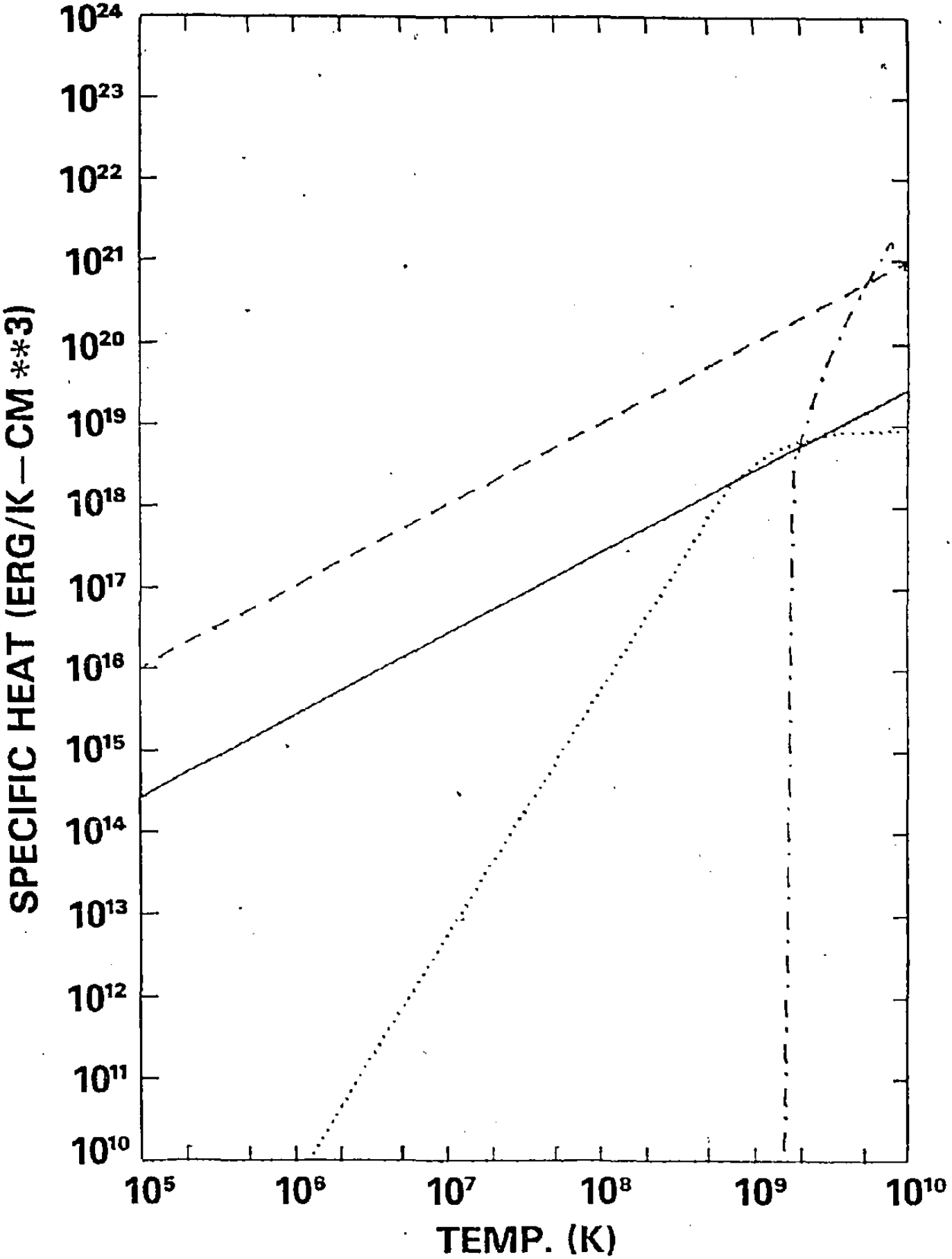
SPECIFIC HEAT (ERG/K—CM **3)
10^24
10^23
10^22
10^21
10^20
10^19
10^18
10^17
10^16
10^15
10^14
10^13
10^12
10^11
10^10
10^5
10^6
10^7
10^8
10^9
10^10
TEMP. (K)

CHAPTER V

NEUTRINO EMISSIVITY

Various nuclear reactions can occur that produce neutrinos (and antineutrinos) without altering the composition of the star. This is the case when a reaction is in equilibrium with its inverse reaction (e.g. β-decay and inverse β-decay). Bremsstrahlung processes that directly convert thermal energy into neutrino-antineutrino pairs also do not alter the composition. Once produced, the neutrinos will escape the star without further interaction (Bahcall and Wolf 1965). (An exception occurs during the first few hours of a neutron star's life, when the neutrino mean free path may be less than the stellar radius, but this is of no consequence later on.)

Following Tsuruta (1978), there are six processes considered here as significant neutrino sources. These are:

i) Beta processes involving pions

$$\pi^- + n \rightarrow n + \mu^- + \bar{\nu}_\mu \qquad (5.1a)$$

$$\pi^- + n \rightarrow n + e^- + \bar{\nu}_e \qquad (5.1b)$$

and their inverse processes

$$n + \mu^- \rightarrow n + \pi^- + \nu_\mu \quad . \tag{5.1c}$$

$$n + e^- \rightarrow n + \pi^- + \nu_e \quad . \tag{5.1d}$$

If pion condensates exist in the star, the above processes will dominate the neutrino emissivity and cool the star very rapidly. This was first pointed out by Bahcall and Wolf (1965).

ii) Modified URCA processes

$$n + n \rightarrow n + p + \mu^- + \bar{\nu}_\mu \tag{5.2a}$$

$$n + n \rightarrow n + p + e^- + \nu_e \tag{5.2b}$$

and their inverse processes

$$n + p + \mu^- \rightarrow n + n + \nu_\mu \tag{5.2c}$$

$$n + p + e^- \rightarrow n + n + \nu_e \quad . \tag{5.2d}$$

Only particles near their Fermi surfaces can partake in these reactions, so an extra spectator particle (neutron) appears on each side of the reaction to allow conservation of momentum and energy.

iii) nn-pair Bremsstrahlung

$$n + n \rightarrow n + n + \nu + \bar{\nu} \tag{5.3}$$

iv) np-pair Bremsstrahlung

$$n + p \rightarrow n + p + \nu + \bar{\nu} \tag{5.4}$$

v) Electron-ion Bremsstrahlung

$$(Z,A) + e^- \rightarrow (Z,A) + e^- + \nu + \bar{\nu} \quad . \tag{5.5}$$

vi) The plasma process

$$\gamma_p \rightarrow \cdot + \bar{\nu} \qquad (5.6)$$

where γ_p is a plasma excitation (plasmon). (This process is not considered by Tsuruta (1978).

For the pion processes (5.1 a-d) Maxwell et al. (1977) have calculated a luminosity

$$nq_\nu^\pi = 1.5\times10^{46}\theta^2 T_9^6 \frac{M}{M_\odot}\frac{\rho_0}{\rho}$$

$$= 2.1\times10^{27}\theta^2 T_9^6 \text{ ergs cm}^{-3}\text{ s}^{-1} . \qquad (5.7)$$

Here T_9 is the temperature in units of 10^9K and θ^2 is a pion density factor. Maxwell et al. (1977) suggest using $\theta^2 = .1$ as a typical value. Also used is a cutoff intensity ρ_π below which there is no pion condensate; ρ_π is treated as a free parameter, although it is expected to fall in the range $(2-20)\times\rho_0$.

The emissivities resulting from processes (ii) to (v) are given by Maxwell (1979).

$$nq_\nu^{URCA} = 1.8\times10^{21}(1+F)\left(\frac{M_N^*}{M_N}\right)^3 \frac{M_p^*}{M_p}\left(\frac{\rho}{\rho_0}\right)^{2/3} T_9^8 \text{ ergs cm}^{-3}\text{s}^{-1} . \qquad (5.8)$$

Here $F = \frac{p_F(n)}{p_F(e)}$, and is included to account for reactions (5.2a) and (5.2c).

$$Nq_\nu^{nn} = 4.4\times10^{19}\cdot\left(\frac{M_N^*}{M_N}\right)^4 \left(\frac{\rho}{\rho_0}\right)^{1/3} T_9^8 \text{ ergs cm}^{-3}\text{s}^{-1} \qquad (5.9)$$

$$nq_\nu^{np} = 5.0\times10^{19} \left(\frac{M_N^*}{M_N}\right)^2 \left(\frac{M_p^*}{M_p}\right)^2 \left(\frac{\rho}{\rho_0}\right)^{2/3} T_9^8 \text{ ergs cm}^{-3}\text{s}^{-1} \quad (5.10)$$

$$nq_\nu^{ions} = 2.1\times10^{20} \frac{Z^2}{A} \frac{\rho}{\rho_0} T_9^6 \text{ ergs cm}^{-3}\text{s}^{-1} . \quad (5.11)$$

The emissivity from the sixth process is given by Maxwell and Soyeur (1979)

$$nq_\nu^{p\ell} = 8.3\times10^{14} \left(\frac{\hbar\omega_{p\ell}}{kT}\right)^{15/2} \exp\left(-\frac{\hbar\omega_{p\ell}}{kT}\right) T_9^9 \text{ ergs cm}^{-3}\text{s}^{-1} \quad (5.12)$$

where the plasma frequency $\omega_{p\ell}$ is related to the chemical potential μ_e by

$$\hbar\omega_{p\ell} = \left(\frac{4\alpha}{3\pi}\right)^{1/2} \mu_e . \quad (5.13)$$

The last two processes take place in the crust (below $\rho = 2\times10^{14}$ g-cm^{-3}), whereas the np-process takes place above 2×10^{14} g-cm^{-3}, where there are free protons.

For evaluating the factor $\frac{Z^2}{A}$ in eqn. (5.11) the results of Negele and Vautherin (1973) are parametrized as:

$$\frac{Z^2}{A} = \max\left[0.2\left(\frac{\rho}{\rho_0}\right)^{-0.61}, 0.62\left(\frac{\rho}{\rho_0}\right)^{-0.37}\right] , \; 1 \leq \frac{Z^2}{A} \leq 10 . \quad (5.14)$$

It is clear from a comparison of the above emissivities that the term nq_ν^π will strongly dominate if a pion condensate is present.

V.1 Superfluidity Effects

The temperature dependent energy gap for nucleon species (i) is approximately

$$\Delta_i(T) = \Delta_i(T=0)\,[1-T/T_c(i)]^{1/2} \quad , \quad T < T_c$$
$$= 0 \qquad\qquad\qquad\qquad\qquad\qquad T > T_c \; . \tag{5.15}$$

$T_c(i)$ and $\Delta_i(T=0)$ are given by Takatsuka (1972).

The emissivities nq_ν^{URCA} and nq_ν^{np} are each reduced by a factor $\exp\{[-\Delta_N(T)-\Delta_p(T)]/T\}$, and nq_ν^{nn} is reduced by a factor $\exp[-2\Delta_N(T)/T]$, from the non-superfluid values (Maxwell 1979).

It is not known how the pion process rate nq_ν^{π} is affected by nucleon superfluidity. The effects of such uncertainties may be accounted for by varying the pion cutoff density ρ_π.

All the above six emissivities are retained since superfluidity may suppress the seemingly dominant ones (such as the URCA process).

CHAPTER VI

RESULTS AND CONCLUSIONS

From the results of the preceeding three chapters, the right hand side of eqn. (2.16) may be evaluated in terms of the 'core temperature' T'. A first order differential equation is thus obtained:

$$\frac{dt}{dT'} = f(T') \quad . \tag{6.1}$$

This may be solved using a simplified Runge-Kutta method:

$$t(T'+\Delta T') = t(T') + \frac{\Delta T'}{6}\{f(T')+4f(T'+\Delta T'/2)+f(T'+\Delta T')\} \tag{6.2}$$

with initial conditions $t = 0$ at $T' = T'_0$. For $T'_0 \gtrsim 5\times10^9$K the choice of starting temperature T'_0 has no effect on the cooling curves, due to the strong temperature dependence of the neutrino luminosity.

The general shape of the cooling curve for a neutron star has been known for some time (Tsuruta 1974, Tsuruta and Cameron 1966) and is clear in Figures (6-1) and (6-2). In the early phase ($t \lesssim 10^4 - 10^5$ years) the cooling is dominated by neutrino emission from the interior, and the slope of the cooling curve in a log T vs log t plot is approximately $-\frac{1}{6}$ (this follows from the heat content of degenerate fermions $\sim T^2$ while the neutrino emissivity $\sim T^8$). This is followed

by a phase of steeper slope in which the cooling is dominated by photon emission from the surface. The change in slope reflects the fact that the photon emission is proportional to the fourth power of the surface temperature, and because, as the star cools, the contrast between the surface and core temperatures is reduced (see Figure 3-2). At temperatures much below 5×10^4 K the star will be isothermal out to the surface, and one expects the cooling curve to have a slope of $-\frac{1}{2}$ (reflecting the T^2 dependence of the heat content and the T^4 dependence of the radiation loss).

Results for the cooling of neutron stars with no magnetic field, but with superfluidity effects accounted for, are presented in Table 6-1 for both equations of state and four stellar masses, at ages appropriate for comparison with young supernova remnants. The variation with mass is not very severe: less than a factor of two for the stiff EOS (PPS), and only 30% for the soft EOS (BPS). For the stiff EOS the most massive stars are the hottest because the specific heat has a stronger density dependence than does the neutrino emissivity, resulting in slower cooling for higher density (more massive) stars. The same is true for the soft EOS models as well, but it is offset in the two most massive cases by the enhancement of neutrino emission by the large central redshift factors (which raise $T = T'e^{-\phi}$). For stars of the same mass, with no pion condensate, the soft EOS model

is the hotter because of the thinner (less insulating) outer layers (see Figure 3-2).

If a pion condensate is present then these models are about a factor of seven cooler, which renders them virtually undetectable as soft x-ray sources. The stiff EOS models have such low central densities that it is unlikely that pion condensates could exist. Whether or not the soft EOS models should have pion condensates is uncertain, as it depends on some poorly known parameters of high density matter. At present, the observed upper limits on the temperatures of putative neutron stars in young supernova remnants are in the range $1\text{-}3\times10^{6}$K (Helfand, Chanin and Novick 1979). As seen in Table 6-1 this is also the expected range of temperature for young neutron stars in the absence of pion condensates. The lack of evidence so far for thermal radiation from neutron stars is suggestive of (but does not demand) the existence of pion condensates in these stars. It would require a lowering of the observed temperature limits by a factor of two to resolve the question satisfactorily.

For reasons discussed in Section III.4, calculations that attempt to incorporate magnetic fields at present have only a qualitative value. The effect of a strong magnetic field is to reduce the opacity and hence the core-surface temperature contrast. In the neutrino-dominated cooling phase this increases the observed (surface) temperature, because

it is the core temperature that controls the cooling rate. However, when the cooling becomes photon-dominated, the lower opacity results in faster heat loss and hence a shorter lifetime. Since the radiation from a cooling magnetized neutron star is expected to be anisotropic (and therefore modulated by stellar rotation), polarization dependent, and deviating in frequency-dependence from black-body radiation , its detection may be less straightforward than in the case of an unmagnetized star.

The effects of nucleon superfluidity are twofold: the specific heat and the neutrino emissivity are both sharply reduced at temperatures below the transition temperature. The result is that the inclusion or exclusion of nucleon superfluidity makes only minor differences in the neutrino-dominated phase. However, in the photon-dominated phase the absent heat content of the superfluid results in a shorter lifetime (see Figures 6-1 and 6-2). This is most pronounced in the low mass, stiff EOS models, for which a substantial mass fraction becomes superfluid. The soft EOS models have only small superfluid regions and so the effects of superfluidity are less noticeable (see Figure 6-1). It is found that the cooling curves are sensitive to the superfluid energy gaps only for ages $\lesssim 10^2$ years, as after that all models are well below plausible transition temperatures.

Lastly, it remains to relate the cooling curves to the possibility of detecting cooling neutron stars. In Figure 6-3 detectability curves (distance vs age) are given for a 1.25 $M_\odot$ neutron star, stiff EOS, with superfluidity included but no magnetic field. The maximum detectable distance at a given age is defined by requiring that the count rate in a 100 cm^2 soft X-ray detector (0.1-4.5 keV) exceed 2.5×10^{-3} counts/sec (modelled on the IPC counter on the Einstein Observatory, see Giacconi et al. 1979). The spectrum is assumed to be blackbody and the three curves are for interstellar densities of 0.3, 1.0 and 3.0 cm^{-3}; the absorption coefficients being those of Brown and Gould (1970). If measurements of this sensitivity were made (as should be possible with the HEAO-II satellite), since Figure 6-3 indicates that the cooling of a number of neutron stars (e.g. the Crab pulsar) should be detectable, then one may be able to select between the various cooling curves and thus learn more about the stars in question.

Table 6-1. Neutron Star Models for Cooling Calculations

EOS	$M/M_\odot$	R(km)	$\rho_{c,14}$	$\bar{\rho}_{14}$	z_s	z_c	T_6 (300 y)	T_6 (1000 y)	ρ_π/ρ_0
BPS	0.4	10.0	6.7	1.90	0.065	0.15	2.45	2.05	-
							0.30	0.27	2
PPS	0.4	17.5	1.7	0.354	0.036	0.088	1.32	1.07	-
BPS	0.7	9.30	13.0	4.13	0.135	0.31	2.72	2.38	-
							0.30	0.27	2
PPS	0.7	16.57	2.5	0.729	0.070	0.155	1.73	1.47	-
BPS	1.25	8.13	27.	11.0	0.35	0.96	2.42	2.13	-
							0.36	0.31	2
PPS	1.25	16.0	3.8	1.45	0.14	0.31	2.10	1.81	-
BPS	1.41	7.00	55.	19.5	0.58	2.36	2.14	1.89	-
							0.36	0.33	2
PPS	1.41	15.75	5.0	1.71	0.167	0.38	2.26	1.94	-
							0.36	0.32	1.5

The equation of state (EOS) is either soft (BPS) or stiff (PPS). The central density, ρ_c, and the mean density, $\bar{\rho}$, are given in units of 10^{14} g-cm^{-3}. Also listed are the surface and central redshifts. The temperature, in units of 10^6 K, is given for each neutron star at ages of 300 y and 1000 y; neutron superfluidity effects are included but magnetic effects are not. The threshold density for the onset of pion condensation is given in units of nuclear matter density, $\rho_0 = 2.8\times10^{14}$ g-cm^3.

Figure 6-1

Cooling curves for a 1.25 $M_\odot$ neutron star with the soft EOS (central density = 2.7×10^{15} g-cm^{-3}). The observed temperature is the gravitationally redshifted surface temperature. There are two sets of four curves each: for the upper set, cooling by a pion condensate is ignored whereas in the lower set this effect is included. Each set divides into two pairs: the pair for which the cooling is ultimately more rapid has a surface magnetic field of 10^{12} G; the other pair corresponds to zero magnetic field. In each pair, the more rapidly cooling curve corresponds to the inclusion of nucleon superfluidity whereas the other member corresponds to its exclusion. The reason for the relatively minor effect of superfluidity is that for this mass and this EOS, the central density is so high that the mass fraction capable of superfluidity is very small.

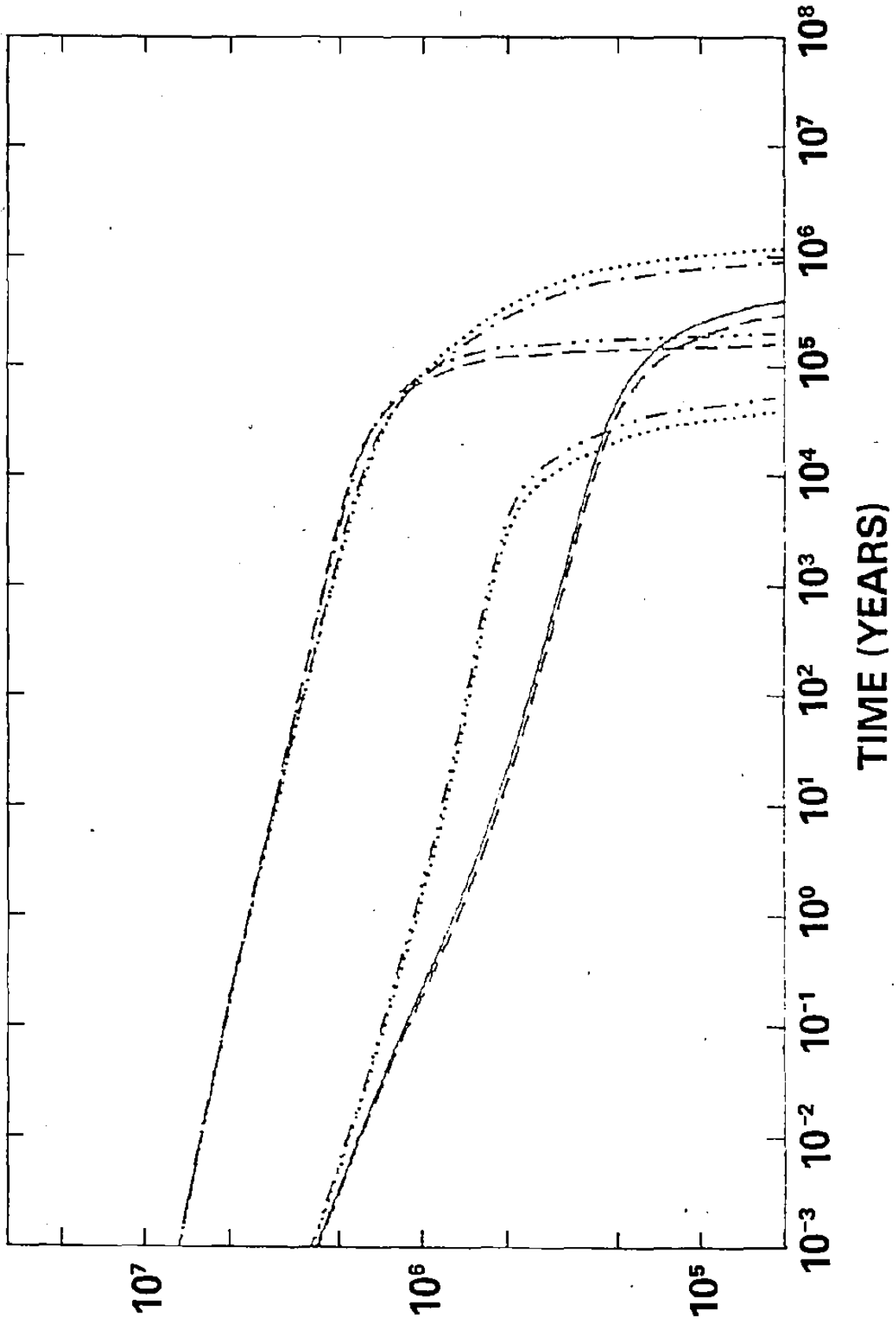
OBS. TEMP. (K)
10^7
10^6
10^5
TIME (YEARS)
10^{-3} 10^{-2} 10^{-1} 10^0 10^1 10^2 10^3 10^4 10^5 10^6 10^7 10^8

Figure 6-1

Figure 6-2

Cooling curves for a 1.25 $M_\odot$ neutron star with the stiff EOS (central density = 3.8×10^{14} g-cm^{-3}). The central density is below that at which it is believed likely for pion condensation to develop, so there are no curves which include the enhanced neutrino cooling effect of a condensate. The two pairs correspond to zero magnetic field (longer lifetime) and a surface field of 10^{12} G (shorter lifetime). At early stages, when neutrino cooling dominates, the effect of a field is to raise the observed surface temperature; at later stages, when photon cooling dominates, the presence of a field then naturally means more rapid cooling. For each pair, one curve has nucleon superfluidity included (and this reduces the lifetime) whereas the other does not. The effect of superfluidity is more pronounced for stars with the stiff EOS (especially those of even lower mass) because a substantial mass fraction is capable of superfluidity.

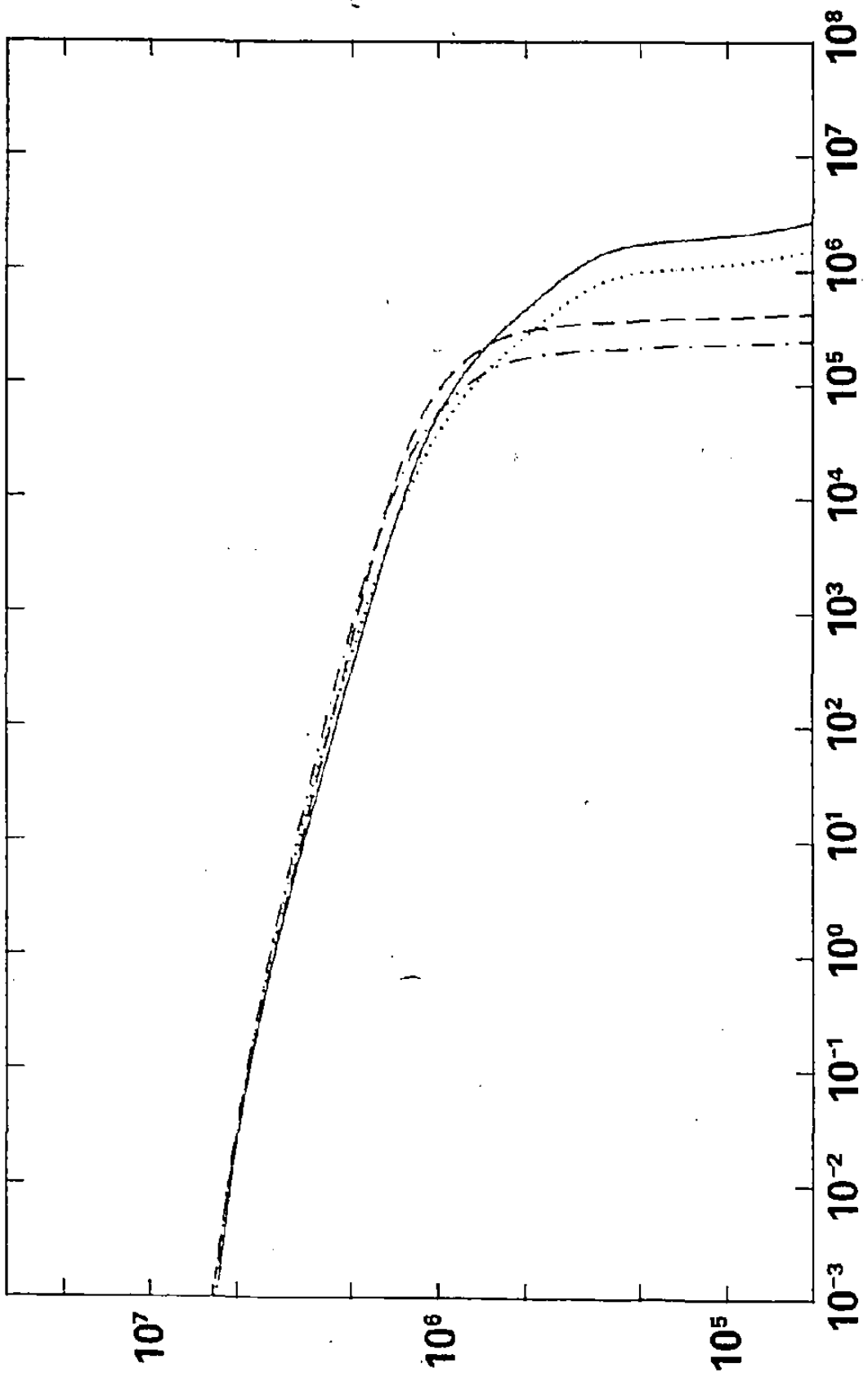
OBS. TEMP. (K)
10^7
10^6
10^5
TIME (YEARS)
10^{-3}
10^{-2}
10^{-1}
10^0
10^1
10^2
10^3
10^4
10^5
10^6
10^7
10^8

Figure 6-2

Figure 6-3

Detectability distance for a 1.25 $M_\odot$ neutron star (stiff EOS, B = 0, neutron superfluidity included) as a function of its age, for a nominal soft X-ray detector of area 100 cm^2, sensitive to X-rays of energy 0.1-4.5 keV. The detectability threshold is taken to be 2.5×10^{-3} counts-s^{-1}. This nominal detector approximately mimics the IPC on HEAO-2. The three curves are for interstellar hydrogen densities of n_H = 0.3, 1.0, and 3.0 cm^{-3}; the X-ray absorption coefficients of Brown and Gould (1970) have been used.

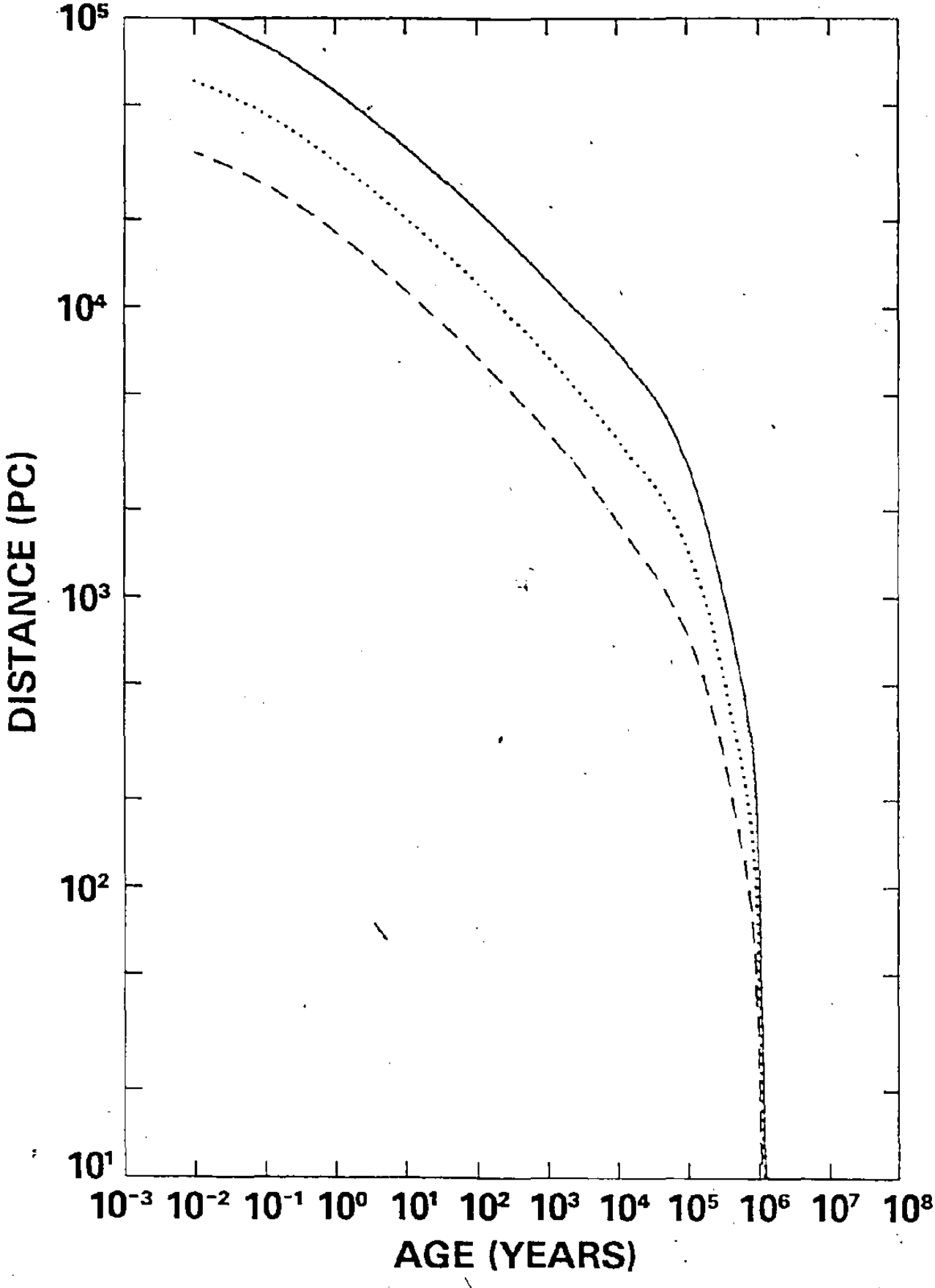
DISTANCE (PC)
10^5
10^4
10^3
10^2
10^1
10^{-3} 10^{-2} 10^{-1} 10^0 10^1 10^2 10^3 10^4 10^5 10^6 10^7 10^8
AGE (YEARS)

Figure 6-3

APPENDIX A

Pressure and Density of a Fermi Gas

The total number of particles is found by integrating over phase space:

$$N = \frac{g}{h^3} \int_0^\infty d^3\underset{\sim}{x} \int_0^\infty d^3\underset{\sim}{p}\ f(\underset{\sim}{p},\underset{\sim}{x}) \ . \qquad (A.1)$$

Here $f(\underset{\sim}{p},\underset{\sim}{x})$ is the distribution function and $g = 2s+1$ is a spin multiplicity factor. For non-interacting spin $\frac{1}{2}$ particles, $g = 2$ and $f(\underset{\sim}{p},\underset{\sim}{x})$ is given by the Fermi distribution

$$f(\underset{\sim}{p},\underset{\sim}{x}) = f(p) = \frac{1}{1+\exp[(\varepsilon-\mu)/kT]} \ . \qquad (A.2)$$

Here $\varepsilon(p)$ is the kinetic energy and μ is the chemical potential. This distribution applies to an electron gas if correlations due to coulomb interactions are negligible.

Integrating over $\underset{\sim}{x}$ and over angles in momentum space:

$$n = \frac{N}{V} = \frac{8\pi}{h^3} \int_0^\infty \frac{p^2 dp}{1+\exp[(\varepsilon-\mu)/kT]} \ . \qquad (A.3)$$

This can be written as a dimensionless energy integral by using

$$cp = \{(\varepsilon + mc^2)^2 - m^2c^4\}^{1/2}, \qquad (A.4)$$

$$c^2 pdp = (\varepsilon+mc^2)\,d\varepsilon \qquad (A.5)$$

and using the definitions

$$\alpha = -\frac{\mu}{kT} , \tag{A.6}$$

$$\beta = \frac{kT}{mc^2} , \tag{A.7}$$

$$x = \frac{\varepsilon}{kT} . \tag{A.8}$$

Eqn. (A.3) then becomes

$$n = \frac{4\rho}{h^3} (2mkT)^{3/2} \int_0^\infty \frac{x^{1/2}(1+\beta x)(1+\frac{1}{2}Bx)^{1/2}dx}{1+e^{\alpha+x}} . \tag{A.9}$$

The matter density is related to the number density of electrons by

$$\rho = \mu_e m_p n$$

where μ_e is the number of nucleons per electron, and m_p is the mass of a nucleon.

For fermions, the thermodynamic potential $\Omega = -PV$ is (see for example Landau and Lifshitz 1958)

$$\Omega = -kT \sum_{\text{states}} \ln(1 + e^{(\mu-\varepsilon)/kT})$$

$$= -kT \frac{g}{h^3} \int d^3x \int d^3p \ln(1 + e^{(\mu-\varepsilon)/kT})$$

$$= -\frac{2kT}{h^3} V 4\pi \int_0^\infty p^2 \ln(1 + e^{(\mu-\varepsilon)/kT}) dp . \tag{A.11}$$

Integrating by parts, one obtains

$$\Omega = -PV = -\frac{8\pi kTV}{h^3} \frac{1}{3} \int_0^\infty \frac{p^3 d\varepsilon}{1+e^{(\varepsilon-\mu)/kT}} . \tag{A.12}$$

Using the definitions (A.6), (A.7) and (A.8), and using equation (A.4), the pressure may be expressed as

$$P = \frac{8\pi kT}{3h^3} (2\pi mkT)^{3/2} \int_0^\infty \frac{x^{3/2}(1 + \frac{1}{2}\beta x)^{3/2} dx}{1 + e^{\alpha+x}} . \quad (A.13)$$

APPENDIX B

RADIATIVE OPACITY IN A MAGNETIC FIELD

Consider waves in an electronic plasma in the presence of an external magnetic field $\underset{\sim}{B}_0$. Neglecting the pressure gradient term, the equation of motion is given by

$$\frac{d\underset{\sim}{v}}{dt} = \frac{\partial \underset{\sim}{v}}{\partial t} + (\underset{\sim}{v}\cdot\nabla)\underset{\sim}{v} = -\frac{e}{m}\left(\underset{\sim}{E} + \frac{1}{c}\,\underset{\sim}{v}\times\underset{\sim}{B}\right) - \gamma\underset{\sim}{v} \qquad (B.1)$$

where γ is the collision frequency. For waves propagating in the z-direction, one expects departures from equilibrium to be of the form $\exp(ikz-i\omega t)$. Therefore:

$$\left.\begin{aligned} \underset{\sim}{B} &= \underset{\sim}{B}_0 + \underset{\sim}{B}_1\, e^{ikz-i\omega t} \\ n &= n_0 + n_1\, e^{ikz-i\omega t} \\ \underset{\sim}{v} &= \underset{\sim}{v}_1\, e^{ikz-i\omega t} \\ \underset{\sim}{E} &= \underset{\sim}{E}_1\, e^{-ikz-i\omega t}. \end{aligned}\right\} \qquad (B.2)$$

The quantities B_1, n_1, v_1 and E_1 are taken to be first order small in comparison to B_0 and n_0.

Putting eqns. (B.2) into eqn. (B.1) and keeping terms only up to first order small, one obtains

$$\underset{\sim}{v} = \frac{-ie}{m(\omega+i\gamma)}\,\underset{\sim}{E} - \frac{ie}{mc(\omega+i\gamma)}\,\underset{\sim}{v}\times\underset{\sim}{B}_0 . \qquad (B.3)$$

Also, from Maxwell's equations and the current density

$$\underset{\sim}{J} = -en\underset{\sim}{v} , \tag{B.4}$$

one obtains, using eqns. (B.2):

$$\underset{\sim}{k}\times\underset{\sim}{E} = \frac{\omega}{c}\underset{\sim}{B}_1 \tag{B.5}$$

$$\underset{\sim}{k}\times\underset{\sim}{B}_1 = \frac{-\omega}{c}\underset{\sim}{E} + i\frac{4\pi en_0}{c}\underset{\sim}{v} . \tag{B.6}$$

Solving the above two equations for $\underset{\sim}{v}$ yields

$$\underset{\sim}{v} = \frac{-ie}{m\omega\omega_p^2}\{c^2(\underset{\sim}{k}\cdot\underset{\sim}{E})\underset{\sim}{k} + (\omega^2-c^2k^2)\underset{\sim}{E}\}, \tag{B.7}$$

where $\omega_p^2 = \frac{4\pi e^2 n_0}{m}$ is the plasma frequency.

Thus, equation (B.3) becomes:

$$(\omega + i\gamma)\{c^2(\underset{\sim}{k}\cdot\underset{\sim}{E})\underset{\sim}{k} + (\omega^2-c^2k^2)\underset{\sim}{E}\}$$
$$= \omega\omega_p^2\underset{\sim}{E} - i\omega_c\{c^2(\underset{\sim}{k}\cdot\underset{\sim}{E})\underset{\sim}{k}\times\hat{B}_0 + (\omega^2-c^2k^2)\underset{\sim}{E}\times\hat{B}_0\}, \tag{B.8}$$

where $\omega_c = \frac{eB}{mc}$ is the cyclotron frequency.

We now look for normal modes of eqn. (B.8) in the two fundamental cases of waves propagating parallel and perpendicular to the magnetic field.

Case (i) $\underset{\sim}{k} \| B_0$

The normal modes are circularly polarized states with $\underset{\sim}{E} = E(\hat{x} \pm i\hat{y})$. For these modes equation (B.8) reduces to

$$(\omega+i\gamma\mp\omega_c)(\omega^2-c^2k^2) = \omega\omega_p^2 \quad . \tag{B.9}$$

Take ω real, k complex, and introduce $\eta^2 = c^2k^2/\omega^2$.

$$\eta^2 = 1 - \frac{\omega_p^2}{\omega(\omega\mp\omega_c+i\gamma)} \quad . \tag{B.10}$$

For $\eta \sim 1$ and $\gamma << \omega$

$$\eta \simeq 1 - \frac{\omega_p^2(\omega\mp\omega_c-i\gamma)}{2\omega(\omega\mp\omega_c)^2} \quad . \tag{B.11}$$

The imaginary part of k results in a damping term of $e^{-\mathrm{Im}(k)z}$. This can be related to the opacity κ as follows:

$$\mathrm{Im}(k) = (\text{mean free path})^{-1} = \kappa\rho \quad . \tag{B.12}$$

Since $\eta = ck/\omega$, the opacities with and without an external magnetic field are related by:

$$\frac{\kappa(B)}{\kappa(B=0)} = \frac{\mathrm{Im}\ \eta(\omega_c)}{\mathrm{Im}\ \eta(\omega_c=0)} = \frac{\omega^2}{(\omega\mp\omega_c)^2} \quad . \tag{B.13}$$

Now, since $\dfrac{\omega^2}{(\omega\mp\omega_c)^2} = \dfrac{\omega^2}{\omega^2+\omega_c^2\mp2\omega\omega_c}$, we take as an approximation

$$\frac{\kappa(B)}{\kappa(B=0)} = \frac{\omega^2}{\omega^2+\omega_c^2} \tag{B.14}$$

valid for both modes in both limits $\omega >> \omega_c$ and $\omega << \omega_c$.

Case (ii) $\underset{\sim}{k} \perp \underset{\sim}{B}_0$

The two normal modes in this case are known as the ordinary and the extraordinary modes.

a) Ordinary mode ($\underset{\sim}{E} || \underset{\sim}{B}_0$)

The ordinary mode is independent of the cyclotron frequency ω_c, so the opacity is unaltered by an external magnetic field.

b) Extraordinary mode ($\underset{\sim}{E} \perp \underset{\sim}{B}_0$)

The dispersion relation for the extraordinary mode becomes

$$(\omega + i\gamma)(\omega^2 - c^2k^2) = \omega\omega_p^2 \left(\frac{\omega^2}{\omega^2+\omega_c^2}\right) . \qquad (B.15)$$

As in case (i) above, the opacity is found from Im(k). In this case one obtains:

$$\frac{\kappa(B)}{\kappa(B=0)} = \frac{\omega^2}{\omega^2+\omega_c^2} , \qquad (B.16)$$

which is identical to eqn. (B.14) for the longitudinal modes.

The above expression (B.16), although not valid for the ordinary mode, is taken as a direction independent opacity for simplicity. Some error is introduced by this, but in any case the simple assumption of a uniform strength mag-

netic field throughout the star is unrealistic and precludes a better quantitative analysis of stars with magnetic fields.

References

Bahcall, J.N., and Wolf, R.A. (1965), Phys. Rev. 140B, 1445.

Baym, G., Pethick, C.J., and Sutherland, P.G. (1971), Ap. J. 170, 299.

Brown, R.L., and Gould,R. (1970), Phys. Rev. D 2, 2252.

Canuto, V., and Chiu, H.-Y. (1969), Phys. Rev. 188, 2446.

Chandrasekhar, S. (1939), An Introduction to the Study of Stellar Structure, (Dover, Chicago), p. 389.

Flowers, E.G., and Itoh, N. (1976), Ap. J. 206, 218.

Giacconi et al. (1979), Ap. J. 230, 540.

Helfand, D.J., Chanan, G.A., and Novick, R. (1979), Columbia Astrophysics Laboratory Contribution No. 174.

Huebner, W.F., Merts, A.L., Magee, N.H. Jr., and Argo, M.F. (1977), Astrophysical Opacity Library, Report #UC-346, Los Alamos Scientific Laboratory, unpublished.

Landau, L.D., and Lifshitz, E.M. (1958), Statistical Physics, 2nd ed., (Addison-Wesley, Reading, Mass.), p. 144.

Lodenquai, J., Canuto, V., Ruderman, M., and Tsuruta, S. (1974), Ap. J. 190, 141.

Manchester, R.N., and Taylor, J.H. (1977), Pulsars, (Freeman, San Francisco).

Maxwell, O.V., Brown, G.E., Campbell, D.K., Dashen, R.F. and Manassah, J.T. (1977), Ap. J. 216, 77.

Maxwell, O.V. (1979), Ap. J. 231, 201.

Maxwell, O.V. and Soyeur, M. (1979), Paper submitted to the 8th International Conference on High Energy Physics and Nuclear Structure, Vancouver, August 13-18.

Negele, J.W., and Vautherin, D. (1973), Nucl. Phys. A207, 298.

Pandharipande, V.R., Pines, D., and Smith, R.A. (1976), Ap. J. 208, 550.

Ruderman, M. (1971), Phys. Rev. Lett. 27, 1306.

Ruderman, M. (1974), in IAU Symposium No. 53, Physics of Dense Matter, ed. C. Hansen, (Reidel, Boston), p. 117.

Takatsuka, T. (1972), Progr. Theor. Phys. 48, 1517.

Thorne, K.S. (1967), in High Energy Astrophysics, lectures given at the Summer School at Les Houches, 1966 (Gordon and Breach, New York), p. 259.

Tsuruta, S., and Cameron, A.G.W. (1966), Can. J. Phys. 44, 1863.

Tsuruta, S. (1974) in IAU Symposium No. 53, Physics of Dense Matter, ed. C. Hansen (Reidel, Boston), p. 209.

Tsuruta, S. (1978), Thermal Properties and Detectability of Neutron Stars - I, Cooling and Heating of Neutron Stars, (Research Institute for Fundamental Physics, Kyoto University, Kyoto).

van Paradijs, J. (1978), Nature 274, 650.

van Paradijs, J. (1979), MIT preprint CSR-HEA-79-3.

Ziman, J.M. (1960), Principles of the Theory of Solids, 2nd. ed., (University Press, Cambridge), p. 144.